Pergamon

Geochimica et Cosmochimica Acta, Vol. 68, No. 1, pp. 31–45, 2004

0016-7037/04 $30.00 + .00

doi:10.1016/S0016-7037(03)00238-2

Experimental study of brucite dissolution and precipitation in aqueous solutions: Surface speciation and chemical affinity control

OLEG S. POKROVSKY* and JACQUES SCHOTT

Géochimie: Transferts et Mécanismes, CNRS (UMR 5563)-OMP-Université Paul-Sabatier, 38, Rue des 36-Ponts 31400 Toulouse, France

(*Received November* 15, 2002; *accepted in revised form March* 26, 2003)

Abstract—Dissolution and precipitation rates of brucite ($Mg(OH)_2$) were measured at 25°C in a mixed-flow reactor as a function of pH (2.5 to 12), ionic strength (10^{-4} to 3 M), saturation index ($-12 < \log \Omega < 0.4$) and aqueous magnesium concentrations (10^{-6} to $5 \cdot 10^{-4}$ M). Brucite surface charge and isoelectric point (pH_{IEP}) were determined by surface titrations in a limited residence time reactor and electrophoretic measurements, respectively. The pH of zero charge and pH_{IEP} were close to 11. A two-pK, one site surface speciation model which assumes a constant capacitance of the electric double layer (5 F/m^2) and lack of dependence on ionic strength predicts the dominance of $>MgOH_2^+$ species at $pH < 8$ and their progressive replacement by $>MgOH°$ and $>MgO^-$ as pH increases to 10–12. Rates are proportional to the square of $>MgOH_2^+$ surface concentration at pH from 2.5 to 12. In accord with surface speciation predictions, dissolution rates do not depend on ionic strength at pH 6.5 to 11. Brucite dissolution and precipitation rates at close to equilibrium conditions obeyed TST-derived rate laws. At constant saturation indices, brucite precipitation rates were proportional to the square of $>MgOH_2^+$ concentration. The following rate equation, consistent with transition state theory, describes brucite dissolution and precipitation kinetics over a wide range of solution composition and chemical affinity:

$$R = k^+_{Mg} \cdot \{ > MgOH_2^+ \}^2 \cdot (1 - \Omega^2)$$

where k^+_{Mg} is the dissolution rate constant, $\{>i\}$ is surface species concentration (mol/m^2), and Ω is the solution saturation index with respect to brucite.

Measurements of nonsteady state brucite dissolution rates, in response to cycling the pH from 12 to 2 (pH-jump experiments), indicate the important role of surface hydroxylation — that leads to the formation of Mg oxo or –hydroxo complexes — in the formation of dissolution-active sites. Replacement of water molecules by these oxygen donor complexes in the Mg coordination sphere has a labilizing effect on the dynamics of the remaining water molecules and thus increases reaction rates.

1. INTRODUCTION

Surface reaction controlled dissolution/precipitation of minerals in aquatic environments is known to regulate the concentration of many elements during weathering processes and migration of pollutants. If many studies have been devoted to the surface chemistry and reactivity of trivalent metal oxides, quartz and aluminosilicates (Amrhein and Suarez, 1988; Wieland et al., 1988; Nagy et al., 1991; Stumm, 1992, 1997; Berger et al., 1994; Dove, 1994; Gautier et al., 1994; Oelkers et al., 1994, 2001; Schott and Oelkers, 1995; Devidal et al., 1997; Kramer and Hering, 1997; Duval et al., 2002), much less attention has been dedicated to divalent metal oxides and silicates (Schott et al., 1981; Schott and Berner, 1983, 1985; Casey, 1991; Wogelius and Walther, 1991; Knauss et al., 1993; Westrich et al., 1993; Oelkers and Schott, 2001) even though the dissolution of Ca-, Mg-, Fe(II)-bearing silicates represents a major contribution to the global cycles of these elements (Berner, 1991). Recently, it has been demonstrated that the chemical nature, hydration state and metal oxygen bond strength of the lattice cations control the overall reactivity of complex Me^{2+}-bearing minerals such as carbonates (Pokrovsky and Schott, 2002) and silicates (Westrich et al., 1993; Velbel, 1999; Pokrovsky and Schott, 2000) in neutral to alkaline solutions. In this regard, studies of pure end-member divalent metal oxides are very timely and useful in breaking down the results of the more complex phases. The present paper is aimed at quantifying the surface-controlled reactivity of magnesium hydroxide (brucite) over a wide range of pH, chemical affinity and ionic strengths.

Brucite is an ideal candidate for investigating dissolution and growth reactions at the solid-solution interface because 1) it has a simple composition and structure and, 2) it can be easily precipitated from supersaturated solutions at ambient temperatures. Important progress has been made in characterizing the surface microtopography and dissolution of periclase (Wogelius et al., 1995; Jordan et al., 1999) and brucite (Jordan and Rammensee, 1996) using X-ray reflectivity measurements and Scanning Force Microscopy. Jordan and Rammensee (1996) showed that brucite dissolution was controlled by reactions occurring at its surface. The main goal of the present work is to use brucite as a model to establish a rigorous relationship between surface speciation and dissolution/precipitation kinetics and to test, for the first time, the coupled effects of chemical affinity and surface speciation on mineral reactivity at close to equilibrium conditions. The second goal is to characterize the reactivity of different sites present at brucite's surface using "pH-jump" experiments. Pioneering "pH-jump" experiments performed by Samson et al. (2000) and Samson and Eggleston

* Author to whom correspondence should be addressed (oleg@lmtg.ups-tlse.fr).

Table 1. Chemical composition of Cedar Hill brucite sample.

Microprobe analyses (average of 11), remainder is water	
oxide	weight %
MgO	66.9
SiO_2	0.13
K_2O	0.0007
CaO	0.011
MnO	0.047
FeO	0.08

ICP-MS analyses			
element	ppm	element	ppm
Al	40	Rb	0.15
Ti	5	Sr	29
V	0.2	Y	0.1
Cr	0.76	Mo	0.51
Ni	48	Cd	0.14
Co	11	Ba	77
Cu	21	La	0.29
Zn	16	Ce	0.12
As	1.4	Pb	6

(1998, 2000) on trivalent metal oxides revealed the important role of hydrolyzed metal sites created at pH $\geq$ 6 on mineral dissolution at acid conditions. To distinguish between the effect on dissolution of protonation/deprotonation and the hydrolysis of surface magnesium sites, several pH-jump experiments have been performed between pH 12 and 2. The results of this study should contribute to a rigorous quantification of the reactivity of various Mg-bearing minerals (silicates, phosphates, fluorides) in a wide range of environmental conditions.

2. MATERIAL AND METHODS

2.1. Brucite Samples

Brucite crystals from Cedar Hill, Pennsylvania were purchased from Ward Scientific Co. X-ray diffraction, ICP-MS, and electron microprobe analyses revealed that these crystals contain less than 0.2% impurities (Table 1). Optically clear crystals ~0.5 cm in size were hand-picked, gently ground with an agate mortar and pestle, and sieved. Two size fractions, 50–100 μm and 100–200 μm, were ultrasonically cleaned in alcohol and dried at 60°C. The specific surface areas of the cleaned powders were 0.204±0.010 and 0.120±0.008 m^2/g, respectively, as determined by krypton absorption using the multi-point B.E.T. method. These powders were used in all kinetic experiments. For surface titration and electrophoretic measurements, brucite powder < 50 μm in size was ground in an agate mortar for 2 h. To eliminate the surface defects produced by grinding, before titration and electrophoresis experiments this powder was aged during 2 d in a pH=10.5 solution under nitrogen atmosphere. The surface area of this powder was 9.2 ± 0.8 m^2/g as measured by N_2 adsorption using the B.E.T. method. Fresh and reacted brucite grains were analyzed using a Jeol JSM840a scanning electron microscope.

2.2. Surface Titration

Because of brucite's high solubility and relatively fast dissolution/precipitation kinetics, batch reactors used for the titration of inert oxides are not suitable. Preliminary titrations of brucite powder in a batch reactor showed that Mg concentration decreases from ~ 0.1 to ~ 10^{-5} M when pH increases from 9 to 12, following the solubility curve and thus making impossible the interpretation of these experiments in terms of surface charge. To overcome these difficulties, a modified limited residence time (LRT) reactor described in Pokrovsky et al. (1999a, 1999b) was used. The volume of the reactor is 5 mL and the residence time of the powder in the reactor varies from 3 to 5 min at pH 9 to 10 and from 0.5 to 1 min at pH $>$ 10.5. Surface titrations were conducted at 25±0.5°C under N_2 atmosphere. Brucite surface area was 450–500 m^2/L and it did not change (within 10%) during surface titration as shown by N_2 B.E.T. surface area measurements of the reacted powder. The solid suspension and supernatant were separately titrated by standardized 0.01–1.00 mol/L HCl or NaOH in the 9 to 12.5 pH range in a background NaCl aqueous solution (0.01 and 1 mol/L). A potential drift of less than 0.5 mV/min at pH $<$ 10.5 and 0.1 mV/min at 10.5 $<$ pH $<$ 12.5 was taken as the steady-state condition for each titration point. Once steady-state was reached, pH was recorded, and a sample taken and immediately filtered and stored for Mg analysis. To assess free hydrogen ion concentrations from pH measurements in highly alkaline solutions, background electrolytes were titrated using the same technique.

2.3. Electrophoretic Measurements

A microelectrophoremeter ("Zetaphoremetre II," model Z3000 SEPHY S.A.R.L.) was used to measure the electrophoretic mobilities and ζ-potentials of brucite particles at 25 ± 1°C. Brucite particles were suspended in aqueous solution (3.0 g/L) for 1 d. For each sample, approximately 30 mL of supernatant (containing solid particles of $<$10-μm grain size) were used to fill the microelectrophoresis cell. Experiments were performed in N_2-saturated solutions of ionic strengths ranging from 0.001 to 0.01 mol/L (NaCl, NaOH), $[Mg^{2+}]_{tot}$ from 10^{-6} to 10^{-4} M, and pH from 9.5 to 11.5. At least three electrophoretic mobility measurements were performed on each sample. The uncertainty ranged from 5 to 20%, being the highest near the isoelectric point. Electrophoretic mobilities were converted to ζ-potentials using the Smoluchowski equation (Hunter, 1989).

2.4. Solution Analysis

Solution pH was measured using a combination glass electrode (Mettler Toledo) calibrated on the activity scale with NBS buffers (pH = 4.006, 6.865, and 9.180 at 25°C). Precision of pH measurements was ± 0.002 U (0.1 mV). In highly alkaline solutions, the electrode was calibrated in terms of free hydrogen concentration obtained by titration of nitrogen-saturated 0.01 and 1.0 mol/L NaCl solutions by standardized 0.1 mol/L NaOH solutions. Total magnesium ($[Mg^{2+}]_{tot}$) concentration was measured by flame atomic absorption using a Perkin Elmer 5100 PC spectrometer equipped with an AS-90 autosampler. High precision of Mg analysis was crucial for surface charge calculations and dissolution rate measurements in Mg-rich solutions (see sections 2.5 and 2.6 below). For these purposes, measurements were performed in triplicate mode, with calibration of four standard solutions after each five samples, with an uncertainty of ±0.5%.

2.5. Surface Charge Computation and the Surface Complexation Model (SCM)

During the titration procedure, the total net surface charge σ_T (mol/m^2) of brucite in solution was calculated following the approach of Charlet et al. (1990) and Pokrovsky et al. (1999a):

$$\sigma_T = \frac{1}{S} \cdot \left(\sum_k z_k [k]_0 - \sum_k z_k [k]_f \right) \quad (1)$$

where S is the surface area of powder in reactor (m^2/L), z_k is the charge of aqueous species k, $[k]_0$ is the calculated concentration (M) of k in this reactor based on the amount of mixed solutions assuming a closed-system and no reaction with the solid phase, and $[k]_f$ stands for its actual concentration computed from the measured pH and $[Mg^{2+}]_{tot}$. Note that the surface charge σ_T is a net excess of charge with reference to that present at the brucite surface in equilibrium with solution where the surface has a conventional zero charge (proton condition, Stumm, 1992). Consequently, the point of zero charge (PZC) of brucite is postulated as the solution composition (pH, [NaCl], $[Mg^{2+}]_{tot}$) when the total net surface charge as determined by Eqn. 1 equals zero. The

Table 2. Surface complexation reactions and their intrinsic stability constants at the brucite - solution interface.

Reaction on the surface	log $K°_{int}$ (25°C, I = 0)
1. $>MgOH° - H^+ = >MgO^-$	-12 ± 0.4
2. $>MgOH° + H^+ = >MgOH_2^+$	10 ± 0.4
EDL capacitance in 0.01 M NaCl	5 ± 1 F/m^2
EDL capacitance in 1.0 M NaCl	5 ± 1 F/m^2
Surface sites density (fixed)	16 μmol/m^2

major uncertainties attached to surface charge calculations stem from the uncertainties on pH (or $[H^+]_{free}$] and $[Mg^{2+}]_{tot}$ measurements at pH > 11.5 and pH < 9.5, respectively. As a result, the actual uncertainties on surface charge values can achieve 30–50% in these pH regions.

The MINTEQA2 computer program (Allison et al., 1991) was used to calculate the equilibrium species distribution in the $Mg(OH)_2$-H_2O-NaCl system. This program combines surface reaction equilibria, homogeneous solution equilibria, and mass balance calculations. The simplest surface speciation model, a single site, two-pK, constant capacitance model (CCM) was used to describe brucite surface charge and isoelectric point and to model brucite's dissolution kinetics. Note that two different types of OH groups are present at brucite surface in aqueous solution. Structural OH layers occur at the (001) surface cleavage but OH/H_2O present at the {hk0} edges originate from the hydration of the low coordinated Mg ions exposed at these surfaces. It is assumed in this study that both surface hydroxyl groups are ampholytes and undergo the same protonation/deprotonation reactions. Following a classic approach for surface speciation modeling of metal oxides, three species were postulated to exist on brucite-water interface: $>MgOH_2^+$, $>MgOH°$ and $>MgO^-$. Formation reactions for these species and their intrinsic constants are listed in Table 2. Parameters of SCM for brucite were obtained by fitting the pH-dependence of surface charge first assuming the same values as for MgO (Sverjensky and Sahai, 1996). Surface site density was fixed at 10 sites/nm^2 like for most oxy(hydr)oxides minerals (Hayes et al., 1991; Sverjensky and Sahai, 1996). A high value of the electric double layer (EDL) capacitance (5 F/m^2) was necessary to model the surface charge measured in this study.

2.6. Dissolution and Precipitation Kinetics

Steady-state dissolution and precipitation rates were obtained at 25.0±0.2°C and distinct solution compositions and pH using a thermostated mixed-flow reactor (Pokrovsky and Schott, 2000). The input fluid was stored under nitrogen in a compressible polyethylene container during the experiments. It was injected into the reactor using a Gilson® peristaltic pump that allows flow rates ranging from 0.05 to 10 mL/min. Brucite dissolution occurred in a 250 mL Azlon® plastic beaker which was continuously stirred with a floating Teflon supported magnetic stirrer. For precipitation experiments, a 30 mL Teflon reactor designed in our laboratory was used. Stirring was controlled by a stirplate located directly beneath the bath. The solution left the reactor through a 1 μm Teflon filter. For several experiments, a combined pH-electrode was fixed into the reactor cover to enable in situ pH measurements. The fluid composition and saturation state with respect to brucite can be regulated by either changing the flow rate or the composition of the inlet solution without dismantling the reactor and/or changing the amount of mineral present during the experiment.

Between 0.5 and 5 g of brucite was allowed to react in fluids of prescribed input compositions. Varying the mass of reacting brucite by a factor of 3 did not change the normalized dissolution rate. No difference between surface-normalized dissolution rate for 50–100 μm and 100–200 μm powder was detected. The change of stirring intensity from ~200 rpm to ~1000 rpm at pH 3 produced an increase of initial-surface normalized dissolution rates by 20–30%. However, the increase of specific surface area due to powder grinding may also contribute to this rate increase with stirring intensity. A steady-state dissolution rate, as indicated by a constant output Mg concentration, was obtained after 2 h to 5 d, depending on the flow rate and reactor volume. For each dissolution rate determination, at least five data points at steady-state conditions were collected. Reacting fluids were comprised of deionized nitrogen-saturated H_2O (MilliQ plus system), Merck reagent grade HCl, NaOH, NaCl, and $MgCl_2$. Special care was taken to avoid contamination of basic solutions by atmospheric CO_2. For this, all solutions were prepared with N_2-saturated water and N_2 bubbling occurred in injected solutions 5 h per day. Analytical control of alkalinity and pH in input solutions did not evidence any contamination by CO_2.

Steady-state reaction rates (R, mol/cm^2/s) were computed from measured solution composition using

$$R = -q \cdot \Delta[Mg^{2+}]_{tot}/s \quad (2)$$

where q (L/s) is the fluid flow rate, $\Delta[Mg^{2+}]_{tot}$ (mol/L) is the concentration of Mg in the input solution minus that in the output solution, and s (m^2) refers to the total mineral surface area.

Uncertainties on the steady-state rate constants given in Tables 3 and 4 are 10–15% and are dominated by the uncertainty on BET surface area measurements (±10%) and the standard deviation of average Mg concentration at steady-state (± 2% at $[Mg^{2+}]_{tot} > 10^{-4}$ M and (± 5–10% at $[Mg^{2+}]_{tot} < 10^{-4}$ M). Repeated dissolution runs performed in solutions of similar composition indicate that dissolution rates do not vary by more than ~10% after elapsed times of greater than 150 h. The uncertainties in the computed surface species concentrations are dominated by the reproducibility of outlet pH concentrations leading to an average error of 0.005 log units. The absolute uncertainties attached to surface species concentrations are substantially larger, however, owing to the uncertainties on the intrinsic surface stability constants (± 0.4 log $K°_{int}$ units). The uncertainties in the computed chemical affinities for the brucite dissociation reaction are due to the uncertainties on the brucite solubility product $K°_{sp}$ (± 0.1 log units, see section 3.2.1. below), $MgOH^+$ association constant (log K = 2.32 ± 0.05 according to Palmer and Wesolowski, 1997), and calculated activity coefficients, but are estimated to be ± 2kJ/mol. These uncertainties are discussed further below.

2.7. "pH-jump" Experiments

These experiments were aimed at measuring transient, non-steady state dissolution rates following fast pH changes ("jumps") from high to low values. The conceptual approach of such experiments has been elaborated by Samson et al. (2000) for trivalent metal oxides. The experiments were performed by changing pH of inlet fluids in the range 12 to 2.5 in 30-mL stirred reactors. Flow rates varied from 5 to 10 mL/min yielding solution residence times of 6 to 3 min. For several experiments, preadjustment of inlet reacting solution was made by acid additions following the method of Samson et al. (2000). A downward pH-jump to pH 2.5 or 3 from neutral to alkaline solutions produced an initial-pH-dependent and reproducible period of elevated brucite dissolution rate that lasted from several tenths of a minute to one hour. Therefore, brucite dissolution rate response to pH-jumps was not connected to the reactor residence time but reflected a gradual change of brucite surface speciation with time following the pH jump. The excess amount of released magnesium during pH-jumps was calculated by measuring the area between the actual outlet concentrations as a function of time and a curve predicted by the mechanical mixing in the reactor followed by steady-state conditions at the final pH. Six experiments lasting ~50 h each were performed. Each pH-jump experiment included between 20 and 40 measurements of Mg concentration and pH. The pH sequences were the following: 9.7-2.7-10.8-2.4; 10.8-2.5-6.5-2.5; 10.1-2.6-6.5-2.6-6.7-2.8; 11.8-2.7-11.8-2.5-11.8-2.5; 10.1-3.2-6.6-2.7; 12.1-6.6-12.1-3.0. In the course of these experiments, the mass of brucite dissolved represented from 30 to 50% of the initial mass of solid. As a result, output Mg concentrations were normalized to the actual amount of solid present in the reactor. This amount was calculated based on total duration of experiments, and measured flow rates and outlet solution concentration.

3. RESULTS AND DISCUSSION

3.1. Surface Chemistry of Brucite

The pH-dependence of brucite ζ-potential (ζ, mV) determined in 0.001 and 0.01 mol/L NaCl/NaOH solutions is pre-

Table 3. Summary of brucite dissolution experiments ($[Mg^{2+}]_{input} = 0$).

Exp #	surface area, m^2	flow rate, mL/min	Duration, h	I, M	pH output	$[Mg^{2+}]$, M output	R, mol/m^2/s	log Ω (saturation index)	$-\log\{>MgOH_2^+\}$, mol/m^2
1-2	0.1007	0.476	43	0.01	10.10	$4.08\cdot10^{-5}$	$3.80\cdot 10^{-9}$	−1.97	5.589
1-3	0.1007	0.240	77	0.01	10.17	$8.40\cdot10^{-5}$	$3.24\cdot 10^{-9}$	−1.52	5.608
1-4	0.1007	0.240	48	0.01	10.15	$8.05\cdot10^{-5}$	$3.31\cdot 10^{-9}$	−1.58	5.603
1-5	0.1007	0.900	62	0.01	10.00	$2.50\cdot10^{-5}$	$2.95\cdot 10^{-9}$	−2.86	5.500
2-4	0.1020	0.440	27	0.01	10.45	$3.30\cdot10^{-5}$	$2.45\cdot 10^{-9}$	−1.53	5.688
2-5	0.1020	0.441	40	0.01	10.62	$2.00\cdot10^{-5}$	$1.38\cdot 10^{-9}$	−1.45	5.739
3-2	0.1003	0.440	40	0.01	11.13	$1.21\cdot10^{-5}$	$8.71\cdot10^{-10}$	−0.498	5.902
3-3	0.1003	0.438	43	0.01	11.46	$5.05\cdot10^{-6}$	$3.63\cdot10^{-10}$	−0.286	6.012
3-4	0.1003	1.71	26	0.01	10.89	$6.60\cdot10^{-6}$	$2.01\cdot10^{-10}$	−1.266	5.824
4-3	0.1044	1.19	39	0.01	9.30	$2.93\cdot10^{-5}$	$5.71\cdot 10^{-9}$	−3.67	5.397
9-1	0.0600	1.76	23	0.01	8.90	$2.20\cdot10^{-5}$	$1.08\cdot 10^{-8}$	−4.63	5.318
9-2	0.0600	0.899	25	0.01	9.13	$2.68\cdot10^{-5}$	$6.76\cdot 10^{-9}$	−4.09	5.362
21-2	0.0600	1.56	24	0.01	9.01	$2.44\cdot10^{-5}$	$1.05\cdot 10^{-8}$	−4.37	5.339
21-3	0.0600	1.53	26	0.01	7.75	$3.01\cdot10^{-5}$	$1.29\cdot 10^{-8}$	−6.90	5.136
21-4	0.0600	1.61	25	0.01	7.05	$3.32\cdot10^{-5}$	$1.49\cdot 10^{-8}$	−8.15	5.050
21-5	0.0600	1.51	28	0.01	6.32	$5.45\cdot10^{-5}$	$2.29\cdot 10^{-8}$	−9.40	4.976
21-6	0.0600	1.51	28	0.01	6.20	$8.45\cdot10^{-5}$	$3.55\cdot 10^{-8}$	−9.45	4.965
27-1′	0.3860	0.950	29	0.01	9.40	$8.79\cdot10^{-5}$	$5.37\cdot 10^{-9}$	−3.03	5.419
28-1′	0.3820	1.02	29	0.01	9.43	$7.90\cdot10^{-5}$	$5.13\cdot 10^{-9}$	−3.02	5.426
40-1	0.120	1.01	22	0.01	9.11	$4.53\cdot10^{-5}$	$6.31\cdot 10^{-9}$	−3.90	5.358
40-3	0.120	0.996	21	0.01	7.21	$1.79\cdot10^{-4}$	$2.51\cdot 10^{-8}$	−7.10	5.069
40-4	0.120	1.01	28	0.01	6.28	$2.25\cdot10^{-4}$	$(3.2 \pm 1.5)\cdot 10^{-8}$	−9.0	4.970
40-5	0.120	1.00	22	0.01	3.31	$5.70\cdot10^{-4}$	$(8 \pm 3)\cdot 10^{-8}$	<-10	4.795
40-6	0.120	4.52	5	0.01	2.54	$1.60\cdot10^{-4}$	$(1.0 \pm 0.4)\cdot 10^{-11}$	<-10	4.800
41-2	0.120	0.975	96	0.001	3.92	$4.14\cdot10^{-4}$	$5.61\cdot 10^{-8}$	<-10	4.790
41-3	0.1816	5.54	12	0.001	3.16	$1.30\cdot10^{-4}$	$6.61\cdot 10^{-8}$	<-10	4.790
18-1	0.0600	0.483	32	0.001	10.82	$9.0\cdot10^{-6}$	$1.20\cdot 10^{-9}$	−1.22	5.800
19-1	0.0600	0.667	32	0.001	10.80	$6.8\cdot10^{-6}$	$1.26\cdot 10^{-9}$	−1.38	5.795
15-1	0.120	0.420	70	0.001	10.79	$3.3\cdot10^{-5}$	$1.93\cdot 10^{-9}$	−0.642	5.792
45-2′	0.1534	1.15	26	0.01	5.23	$2.66\cdot10^{-4}$	$3.31\cdot 10^{-8}$	−10.8	4.888
45-3″	0.1534	0.734	28	0.01	5.60	$3.95\cdot10^{-4}$	$3.16\cdot 10^{-8}$	−10.5	4.915
47-1′	0.1534	0.989	18	0.01	5.06	$4.32\cdot10^{-4}$	$4.68\cdot 10^{-8}$	−10.9	4.876
47-2′	0.1534	0.988	28	0.01	4.59	$5.33\cdot10^{-4}$	$5.75\cdot 10^{-8}$	−12.0	4.847
42-3	0.5980	1.12	24	0.01	6.71	$8.78\cdot10^{-4}$	$2.74\cdot 10^{-8}$	<-0.5	N.D.
42-4	0.5980	1.15	15	0.03	6.60	$8.20\cdot10^{-4}$	$2.63\cdot 10^{-8}$	<-0.5	N.D.
42-5	0.5980	1.20	11	0.1	6.71	$8.26\cdot10^{-4}$	$2.75\cdot 10^{-8}$	<-0.5	N.D.
42-6	0.5980	1.20	23	0.3	6.75	$7.86\cdot10^{-4}$	$2.63\cdot 10^{-8}$	<-0.5	N.D.
42-7	0.5980	1.23	23	1.0	6.70	$5.95\cdot10^{-4}$	$2.04\cdot 10^{-8}$	<-0.5	N.D.
42-8	0.5980	1.25	24	3.0	6.44	$6.88\cdot10^{-4}$	$2.40\cdot 10^{-8}$	<-0.5	N.D.
9-3	0.0600	0.900	33	0.05	9.13	$2.45\cdot10^{-5}$	$6.17\cdot 10^{-9}$	<-0.5	N.D.
9-4	0.0600	0.895	40	0.1	9.22	$2.45\cdot10^{-5}$	$6.17\cdot 10^{-9}$	<-0.5	N.D.
10-2	0.0600	0.860	25	0.001	9.13	$2.83\cdot10^{-5}$	$6.76\cdot 10^{-9}$	<-0.5	N.D.
10-3	0.0600	0.830	32	0.002	9.15	$2.98\cdot10^{-5}$	$6.92\cdot 10^{-9}$	<-0.5	N.D.
10-4	0.0600	0.814	40	0.005	9.13	$2.40\cdot10^{-5}$	$6.31\cdot 10^{-9}$	<-0.5	N.D.
11-2	0.0600	0.868	25	$5\cdot10^{-5}$	9.12	$2.62\cdot10^{-5}$	$6.31\cdot 10^{-9}$	<-0.5	N.D.
11-3	0.0600	0.842	32	0.2	9.20	$2.80\cdot10^{-5}$	$6.61\cdot 10^{-9}$	<-0.5	N.D.
11-4	0.0600	0.864	40	0.5	9.15	$3.00\cdot10^{-5}$	$7.24\cdot 10^{-9}$	<-0.5	N.D.
12-1	0.0600	0.445	54	0.001	11.14	$7.52\cdot10^{-6}$	$9.12\cdot10^{-10}$	<-0.5	N.D.
12-2	0.0600	0.442	60	0.005	11.12	$7.00\cdot10^{-6}$	$8.51\cdot10^{-10}$	<-0.5	N.D.
12-3	0.0600	0.448	60	0.02	10.92	$6.45\cdot10^{-6}$	$7.94\cdot10^{-10}$	<-0.5	N.D.
12-4	0.0600	0.450	70	0.1	10.95	$7.49\cdot10^{-6}$	$9.33\cdot10^{-10}$	<-0.5	N.D.
12-5	0.0600	0.451	72	0.5	10.89	$6.71\cdot10^{-6}$	$8.32\cdot10^{-10}$	<-0.5	N.D.

N.D. = Not Determined. Ionic strength is adjusted by NaCl/HCl/NaOH addition

sented in Figure 1. The pH of the isoelectric point was found to be around 11 which is in good agreement with electrophoretic measurements of Schott (1981) who reported pH_{IEP}=10.8. Within the framework of the one-site, two-pK SCM used in this study (Table 2), this implies that $(pK_1+pK_2)/2 = 11$ consistent with $pK_1 = 10$ and $pK_2 = 12$ similar to MgO (Sverjensky and Sahai, 1996).

Results of brucite surface charge determinations in 0.01 mol/L and 1.0 mol/L NaCl are shown in Figure 2. The surface charge decreases linearly with increasing pH with a point of zero charge around 11. The solid line in Figure 2 is the theoretical surface charge calculated using MINTEQA2 code with SCM parameters given in Table 2. From the fitting of experimental data, maximal uncertainties of ± 0.4 log units and

Table 4. Summary of brucite dissolution/precipitation rates measured at 25°C in mixed-flow reactor system at close-to-equilibrium conditions. Negative rates mean precipitation.

No	surface area, m^2	duration, h	flow rate, mL/min	I,M	pH	$[Mg^{2+}]$, M input	$[Mg^{2+}]$, M output	Rate, $mol/m^2/s$	log Ω (saturation index)	$-\log\{>MgOH_2^+\}$, mol/m^2
5-1	0.1018	52	0.892	0.01	11.70	0	$1.35\cdot10^{-6}$	$1.97\cdot10^{-10}$	−0.399	6.093
5-2	0.1018	40	0.446	0.01	11.70	0	$1.74\cdot10^{-6}$	$1.26\cdot10^{-10}$	−0.303	6.093
5-3	0.1018	65	0.422	0.01	11.80	$4\cdot10^{-7}$	$1.90\cdot10^{-6}$	$1.03\cdot10^{-10}$	−0.095	6.127
5-4	0.1018	81	0.210	0.01	11.86	0	$1.80\cdot10^{-6}$	$6.03\cdot10^{-11}$	−0.039	6.147
5-5	0.1018	89	0.206	0.01	11.87	$1.24\cdot10^{-6}$	$1.80\cdot10^{-6}$	$1.91\cdot10^{-11}$	−0.024	6.150
6-2	0.1018	51	0.420	0.01	10.98	0	$1.54\cdot10^{-5}$	$1.05\cdot10^{-9}$	−0.727	5.853
16-1	0.120	70	0.215	0.002	11.20	$2\cdot10^{-7}$	$5.85\cdot10^{-6}$	$1.75\cdot10^{-10}$	−0.562	5.925
17-1	0.120	70	0.184	0.003	11.46	0	$4.5\cdot10^{-6}$	$1.26\cdot10^{-10}$	−0.219	6.012
17-4	0.120	90	0.200	0.003	11.44	$7.89\cdot10^{-6}$	$5.69\cdot10^{-6}$	$-6.12\cdot10^{-11}$	−0.009	6.00
17-5	0.120	372	0.080	0.003	11.41	$8.05\cdot10^{-6}$	$5.46\cdot10^{-6}$	$-2.90\cdot10^{-11}$	−0.051	5.99
37-1	0.5586	38	0.736	0.01	11.32	0	$1.89\cdot10^{-6}$	$1.74\cdot10^{-10}$	−0.783	5.965
37-3	0.120	93	0.192	0.01	11.30	$1.63\cdot10^{-5}$	$1.53\cdot10^{-5}$	$-2.70\cdot10^{-11}$	−0.026	5.958
37-4	0.120	110	0.190	0.01	11.29	$3.20\cdot10^{-5}$	$2.50\cdot10^{-5}$	$-1.86\cdot10^{-10}$	0.263	5.950
38-1	0.120	38	0.745	0.01	11.76	0	$1.42\cdot10^{-6}$	$1.48\cdot10^{-10}$	−0.296	6.113
38-2	0.120	81	0.195	0.01	11.80	0	$1.88\cdot10^{-6}$	$5.13\cdot10^{-11}$	−0.100	6.120
38-3	0.120	93	0.192	0.01	11.76	$6.19\cdot10^{-6}$	$2.14\cdot10^{-6}$	$-1.09\cdot10^{-10}$	0.344	6.113
38-4	0.120	110	0.190	0.01	11.80	$6.68\cdot10^{-6}$	$1.93\cdot10^{-6}$	$-1.26\cdot10^{-10}$	0.439	6.128
39-3	0.120	93	0.220	0.01	12.09	$6.55\cdot10^{-6}$	$3.92\cdot10^{-6}$	$-8.1\cdot10^{-11}$	0.650	6.225
39-4	0.120	110	0.212	0.01	12.12	$6.94\cdot10^{-6}$	$1.00\cdot10^{-6}$	$-7.8\cdot10^{-11}$	0.095	6.230
27-1	0.864	46	0.629	0.01	9.78	$1.01\cdot10^{-5}$	$3.63\cdot10^{-5}$	$3.18\cdot10^{-9}$	−2.50	5.527
27-3	0.864	90	0.612	0.01	10.16	$5.06\cdot10^{-4}$	$5.25\cdot10^{-5}$	$(2.3\pm0.5)\cdot10^{-9}$	−1.37	5.606
7-1	0.1018	27	0.990	0.01	10.78	0	$1.62\cdot10^{-5}$	$2.10\cdot10^{-9}$	−1.09	5.795
7-2	0.1018	50	0.350	0.01	10.73	0	$2.20\cdot10^{-5}$	$1.90\cdot10^{-9}$	−1.05	5.773
7-3	0.1018	60	0.402	0.01	10.78	$1.59\cdot10^{-4}$	$1.69\cdot10^{-4}$	$6.61\cdot10^{-10}$	−0.071	5.795
7-4	0.1018	96	0.200	0.01	10.80	$1.63\cdot10^{-4}$	$1.73\cdot10^{-4}$	$3.31\cdot10^{-10}$	−0.022	5.795
29-2	0.1180	60	0.392	0.01	10.97	$9.75\cdot10^{-5}$	$9.03\cdot10^{-5}$	$-4.00\cdot10^{-10}$	0.025	5.849
29-3	0.1180	76	0.390	0.01	10.87	$1.71\cdot10^{-4}$	$1.64\cdot10^{-4}$	$-3.85\cdot10^{-10}$	0.107	5.817
29-4	0.5900	110	0.384	0.01	10.88	$1.65\cdot10^{-4}$	$9.10\cdot10^{-5}$	$-(8\pm3)\cdot10^{-10}$	0.111	5.820
28-1	0.904	33	0.665	0.01	10.62	$5.07\cdot10^{-5}$	$6.70\cdot10^{-5}$	$2.00\cdot10^{-9}$	−0.781	5.739
28-2	0.904	45	0.664	0.01	10.54	$5.58\cdot10^{-5}$	$7.00\cdot10^{-5}$	$1.74\cdot10^{-9}$	−0.918	5.715
28-6	0.904	47	0.654	0.01	11.05	$4.00\cdot10^{-5}$	$4.35\cdot10^{-5}$	$4.45\cdot10^{-10}$	−0.139	5.875
26-1	0.120	28	0.913	0.001	10.48	$1.84\cdot10^{-4}$	$2.00\cdot10^{-4}$	$1.97\cdot10^{-9}$	−0.476	5.697
26-3	0.120	42	0.645	0.001	10.02	$5.15\cdot10^{-4}$	$5.53\cdot10^{-4}$	$3.41\cdot10^{-9}$	−0.905	5.568
26-4	0.120	50	0.645	0.001	9.94	$1.01\cdot10^{-3}$	$1.04\cdot10^{-3}$	$2.82\cdot10^{-9}$	−0.810	5.547
58-1	0.2620	52	0.187	0.001	10.85	0	$9.20\cdot10^{-5}$	$1.09\cdot10^{-9}$	−0.085	5.811
58-2	0.2620	68	0.186	0.001	10.87	$3.75\cdot10^{-4}$	$1.49\cdot10^{-4}$	$-(2.7\pm0.1)\cdot10^{-9}$	0.159	5.817
58-3	0.2620	66	0.190	0.001	10.74	$2.73\cdot10^{-4}$	$2.00\cdot10^{-4}$	$-(1.0\pm0.1)\cdot10^{-9}$	0.039	5.776
58-4	0.2620	72	0.189	0.001	10.63	$3.73\cdot10^{-4}$	$3.21\cdot10^{-4}$	$-(6.3\pm2.5)\cdot10^{-10}$	0.027	5.742
59-1	0.2620	52	0.226	0.005	11.65	0	$4.50\cdot10^{-6}$	$5.75\cdot10^{-11}$	0.028	6.076
59-2	0.2620	68	0.220	0.005	11.74	$7.76\cdot10^{-6}$	$3.80\cdot10^{-6}$	$-(5.5\pm1.0)\cdot10^{-11}$	0.176	6.106
59-3	0.2620	66	0.220	0.005	11.80	$9.56\cdot10^{-6}$	$3.62\cdot10^{-6}$	$-8.3\cdot10^{-11}$	0.216	6.127
59-4	0.7860	72	0.221	0.005	11.86	$1.79\cdot10^{-5}$	$3.32\cdot10^{-6}$	$-6.83\cdot10^{-11}$	0.267	6.147

Ionic strength is adjusted by NaCl/NaOH addition

$\pm$ 1 F/m^2 can be attributed to the values of surface site stability constants and EDL capacitance, respectively. The effect of ionic strength on surface charge is almost negligible compared to oxide minerals. A possible explanation for this behavior is that the high uncertainties attached to surface charge measurements far from pH_{PZC} can mask the actual differences of σ values for different ionic strengths. However, it is worth noting that a weak dependence of surface charge on ionic strength has been reported for other alkali-earth bearing minerals such as magnesite (Pokrovsky et al., 1999a) or dolomite (Pokrovsky et al., 1999b). Accordingly, high capacitance of the electric double layer has been invoked to describe the surface charge of various Ca- and Mg-bearing minerals (Wu et al., 1991, Van Cappellen et al., 1993; Pokrovsky et al., 1999a, 1999b). Other sheet minerals such as kaolinite are also characterized by EDL capacitance of several F/m^2 (Huertas et al., 1998). The high value of EDL capacitance and its weak dependence on ionic strength is consistent with a thin and highly structured (i.e., non-diffuse) double layer capable of accommodating high charge densities. Whether this is a characteristic feature of all alkaline-earth bearing minerals or merely an experimental artifact in surface charge measurements for highly reactive minerals is not possible to assess solely from the results of the present study. Direct observations of brucite-solution interface structure at an atomic level similar to those performed for calcite (Fenter et al., 2000) could help to resolve this problem.

The dominant species at the $Mg(OH)_2 - H_2O$ interface are $>MgOH_2^+$ and $>MgOH°$ as illustrated by the speciation diagram presented in Figure 3. Concentration of $>MgOH_2^+$ stays almost constant at $pH < 5$ but decreases abruptly at $pH > 8$. The concentration of the deprotonated Mg sites $>MgO^-$ becomes significant only at $pH > 12$.

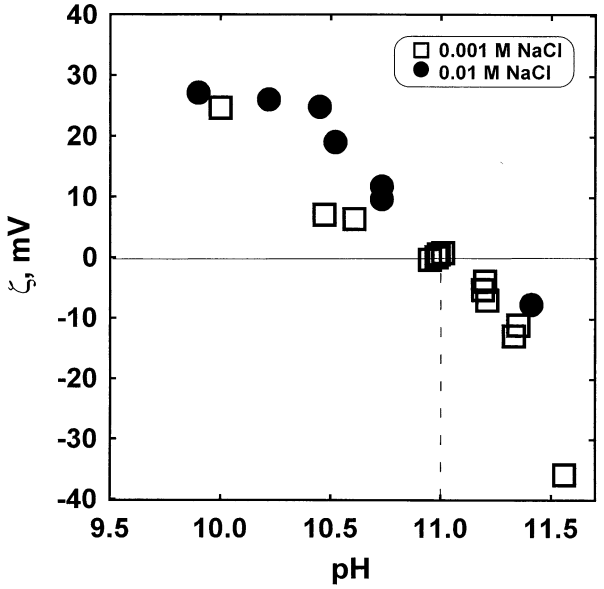

Fig. 1. Influence of pH on brucite ζ-potential at 25°C in 0.001 mol/L NaCl (open squares) and 0.01 mol/L NaCl (closed circles). The dashed line denotes the pH of the isoelectric point.

3.2. Steady-State Dissolution and Precipitation Kinetics

Results of 94 steady-state dissolution/precipitation experiments performed at $2.5 \leq pH \leq 12.2$ are listed in Tables 3 and 4. Included in these tables are reacting solid surface area, fluid flow rates, outlet fluid pH, $[Mg^{2+}]_{tot}$, saturation indices, concentrations of surface species at the brucite - solution interface, and steady-state brucite dissolution and precipitation rates. The surface area used to calculate the rates listed in Tables 3 and 4 was that measured on the fresh (unreacted) brucite powder

3.2.1. Dissolution and precipitation rates as a function of solution composition

3.2.1.1. Influence of pH and ionic strength on dissolution rates. Brucite steady-state dissolution rates measured at 25°C in 0.01 mol/L NaCl solutions are depicted as a function of pH in Figure 4. It can be seen that the rate data define two distinct pH regions. In neutral to acid solutions (pH≤8), rates weakly depend on pH with a log R – pH slope of ~ -0.2. In alkaline solutions (pH $>$ 8), rates decrease abruptly with a slope of -0.5 to -1. Dissolution rates measured at pH $>$ 11.5 are always affected by the influence of chemical affinity which yields the apparent scatter of data observed in this region.

Brucite dissolution rates measured at pH 6.5, 9.2 and 11 as a function of ionic strength (I) are shown in Figure 5. It can be seen that dissolution rates do not depend on I between 0.001and 1–3 mol/L NaCl. It is worth noting that only a weak dependence of dissolution rates on I has been reported for other Mg-bearing minerals such as magnesite and dolomite (Pokrovsky et al., 1999b; Pokrovsky and Schott, 1999) and forsterite (Pokrosky and Schott, 2000).

3.2.1.2. Effect of chemical affinity and the solubility product of brucite. The saturation index of reacting solution with respect to brucite is defined as

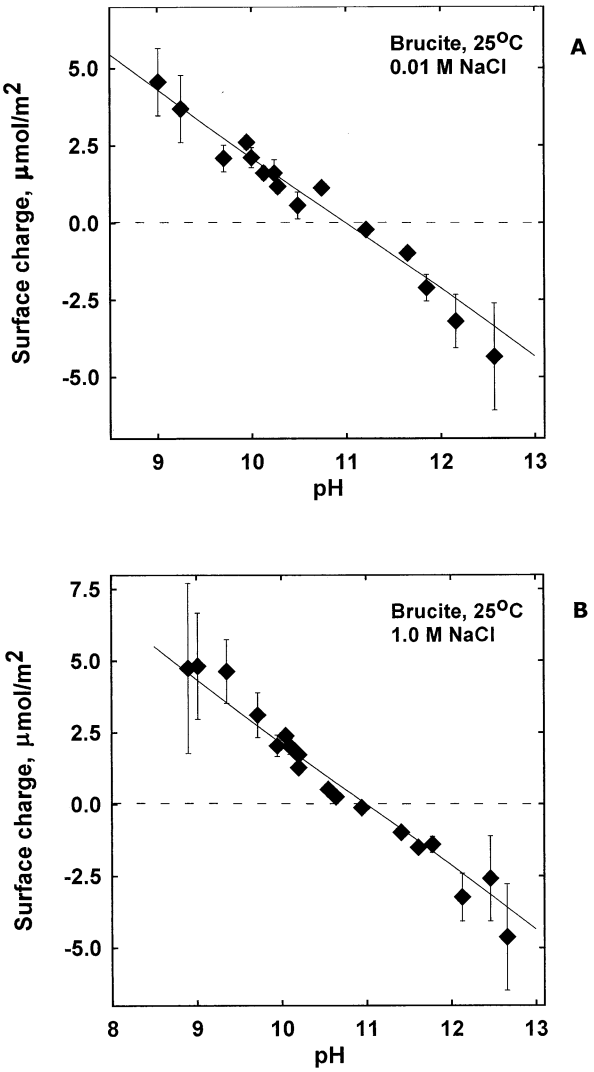

Fig. 2. Surface charge of brucite in aqueous solution determined by acid/base titration in a limited residence time reactor at 25°C in 0.01 mol/L NaCl (A) and 1.0 mol/L NaCl (B). Fit of data (solid lines) was made using the surface complexation model generated in this study.

$$\Omega_{Mg(OH)_2} = \frac{a_{Mg^{2+}} \cdot a^2_{OH^-}}{K^\circ_{sp}} \quad (3)$$

where a_i is the activity of i-th ion in aqueous solution and K°_{sp} is the equilibrium constant for brucite dissociation reaction

$$Mg(OH)_2(s) = Mg^{2+}(aq) + 2OH^-(aq) \quad (4)$$

Close to equilibrium, brucite dissolution rates decrease sharply with chemical affinity (Fig. 6a,b) whereas distinct precipitation occurs in solutions supersaturated with respect to this mineral. Surface-normalized precipitation rates are reproducible and do not depend on powder grain size and intensity of stirring. The brucite solubility product (pK°_{sp}) deduced from dissolution/crystallization rates measured at pH $<$ 11 and 11 $<$ pH $<$ 12.1 at 25°C was found equal to 10.35 $\pm$ 0.05 and 10.45 $\pm$ 0.05, respectively, thus yielding a mean value of $pK^\circ_{sp} = 10.40 \pm$

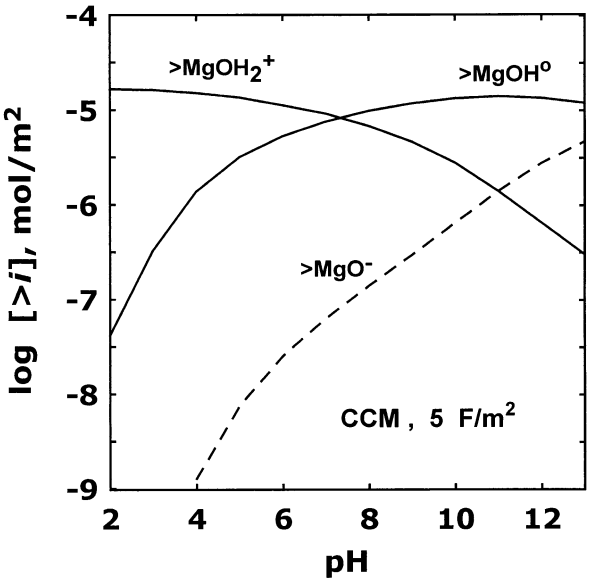

Fig. 3. Calculated surface speciation of brucite in 0.01 mol/L NaCl using a 2 pK, constant capacitance SCM.

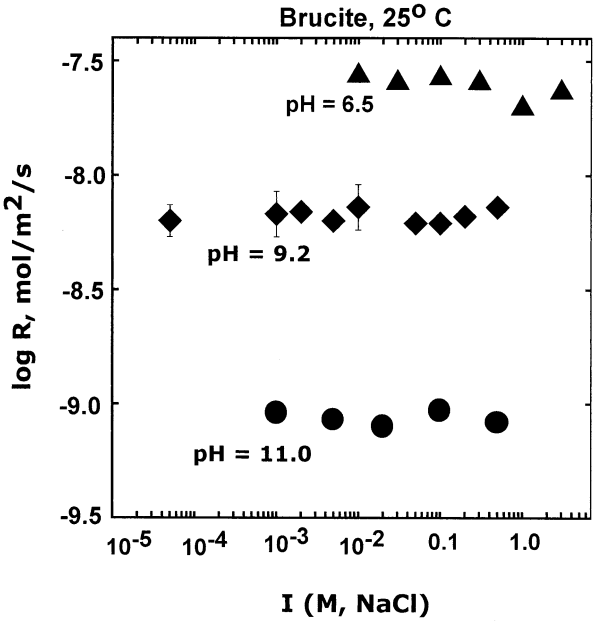

Fig. 5. The effect of ionic strength on brucite dissolution rate at pH 6.5 to 11.0.

0.05. This value has been further confirmed in this study via pH and $[Mg^{2+}]_{tot}$ measurements in 0.01 mol/L and 1.0 mol/L NaCl solutions equilibrated with a brucite powder of high surface area (500 m^2/L). An average $pK°_{sp} = 10.5 \pm 0.2$ was deduced from these experiments which is in good agreement with measurements of natural and synthetic brucite solubility in freshwater and seawater (Pokrovsky and Savenko, 1992). Values of brucite solubility product reported in the literature range between $10^{-10.50}$ and $10^{-11.20}$ (Hostetler, 1963; Liu and Nancollas, 1973). Recently, a detailed study of brucite solubility in $MgCl_2$ solutions using a liquid junction free cell has been performed by Altmaier et al. (in press). These authors recommended $pK°_{sp} = 10.9 \pm 0.2$. However, the solubility product of freshly precipitated crystalline brucite is an order of magnitude higher (Klein et al., 1967; Liu and Nancollas, 1973). The presence in our sample of submicron particles and crystal defects produced by prolonged grinding and the higher solubility of brucite precipitated in kinetic experiments may be responsible for the slight difference between brucite $pK°_{sp}$ value determined in this study and that recommended by Altmaier et al. (2003).

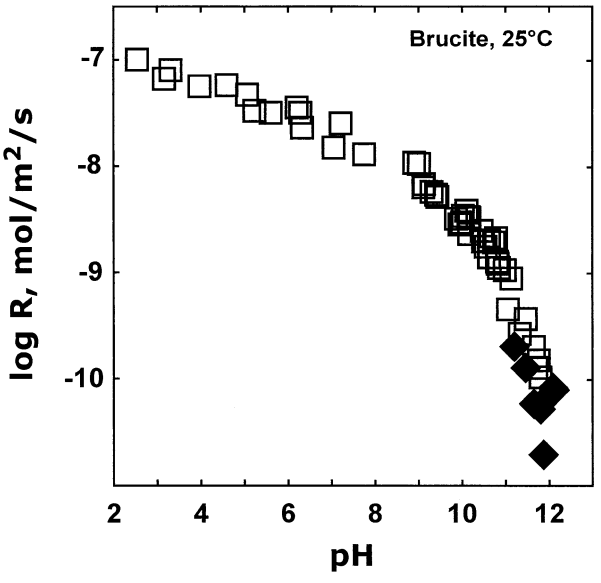

Fig. 4. Summary of brucite steady-state dissolution rates at 25°C as a function of pH in 0.01 mol/L NaCl solutions. The solid symbols represent rates measured at close to equilibrium conditions ($\Omega > 0.5$) where the effect of chemical affinity is significant. The error bars for this and other figures are within the size of data points unless shown.

3.2.1.3. Change of specific surface area during experiments. SEM observations showed that the surface of reacted grains is similar to that of the fresh powder although some fine particles might be present on terraces (Fig. 7a,b). For acid-reacted grains (Fig. 7c) the amount of trigonally arranged dissolution steps on (001) basal surfaces increased as dissolution proceeded via retreat of steps on terraces parallel to the surface (Jordan and Rammensee, 1996). In contrast, the appearance of edge surfaces does not differ between fresh powders, neutral and acid-reacted grains (not shown). This may indicate a low reactivity of edges compared to (001) planes although a special high-resolution microscopic study would be necessary to confirm this hypothesis. In alkaline supersaturated solutions, the surface looks like it is covered with precipitate (Fig. 7d).

The change of the specific surface area (SA) of reacted grains after dissolution/precipitation experiments was followed by B.E.T surface measurements (Table 5). In precipitation experiment No 29-4, SA increased by a factor of 5, but in most experiments lasting >48 h, SA increased by a factor of 1.5 to 3 independently of rate values, solution pH, and saturation index with respect to brucite. At the same time, the flux of

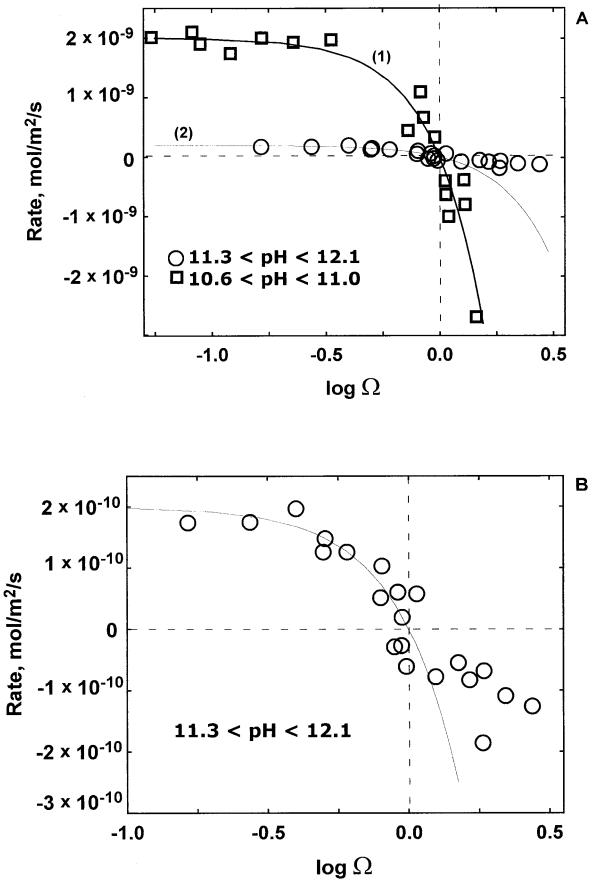

Fig. 6. Brucite overall reaction rate as a function of saturation index for I = 0.01–0.001 mol/L and various pHs. Lines 1 and 2 are calculated using Eqn. 15 with $n = 2$ and $K°_{sp} = 10^{-10.40\pm0.1}$. Bottom figure shows an enlargement of top figure for experiment performed at $11.3 < pH < 12.1$.

dissolved or precipitated magnesium normalized to original SA remains constant within ±10%.

3.2.1.4. Comparison with literature data. A fairly large amount of studies has been devoted to brucite and periclase (MgO) dissolution (Macdonald and Owen, 1971; Sangwal and Arora, 1978; Jones et al., 1981, 1984; Jordan and Rammensee, 1996; Berry et al., 1998; Monastra and Grandstaff, 1999; Morth and Strandh, 1999) and magnesium hydroxide precipitation kinetics (Klein et al., 1967; Liu and Nancollas, 1973; Phillips et al., 1977; Chieng and Nancollas, 1982; Tsuge et al., 1997); some of them are summarized in Figure 8. The study of natural and synthetic brucite dissolution in a batch reactor performed by Vermilyea (1969) revealed a strong dependence of rates on pH and found an activation energy of 42 kJ/mol consistent with a surface-controlled reaction. Recently, Jordan and Rammensee (1996) showed, using Scanning Force Microscopy, that the dissolution of brucite at pH 2.7 and 25°C is surface controlled with an activation energy of 60 kJ/mol, whereas Morth and Strandh (1999), using a rotating disk reactor, argued for a mixed surface/transport control of dissolution at pH of 1.7 to 4.7. Weak dependence of dissolution rate on stirring rates observed in the present study likely indicates that surface chemical reaction rather than transport in solution controls brucite dissolution process. For MgO or $Mg(OH)_2$, most authors (Vermiliya, 1969; Segall et al., 1978; Jordan et al., 1999) agree that the order of dissolution rate with respect to pH is close to −0.5. However, Jones et al. (1981) reported for MgO pH-independent rates at $2 < pH < 4$ and Monastra and Grandstaff (1999) argued for −0.07 rate order. The differences between MgO and $Mg(OH)_2$ dissolution rates measured by different authors can achieve several orders of magnitude (Fig. 8). Most investigators quantified reaction rates by monitoring H^+ consumption during dissolution without measuring the flux of dissolved magnesium. The Mg release-based dissolution rate of brucite powder measured in the present study at pH 2.5 - 3.0 is ~ 5 times lower than the value reported by Jordan and Rammensee (1996) for the (001) surface from direct microscopic measurements of step migration rate in a flow-through cell. However, normalization of measured rates to surface area of reacted solid presents a serious problem for direct comparison between the results of different measurements. For example, it is possible that the corners of brucite crystals, which represent a significant part of total surface area for powders, are less reactive than the terraces. With regard to precipitation rates, comparison of data from different sources is rather difficult as pH of solutions and specific surface area were not reported and constant supersaturation rarely has been maintained during experiments. In a constant composition study of Chieng and Nancollas (1982), surface limited precipitation was observed with a reaction order with respect to saturation from 3 to 7 whereas Liu and Nancollas (1973) argued for a first-order dependence of crystallization rate on Ω at pH ~ 10.8.

3.2.2. *Dissolution and precipitation rates as a function of surface speciation*

3.2.2.1. Dissolution at far from equilibrium conditions. In accord with the surface coordination approach for oxy(hydr)oxide minerals, the increase of brucite dissolution rate with decreasing pH is due to protonation reactions occurring at the mineral surface (Stumm and Wieland, 1990). Within the TST/surface complexation approach, the proton-promoted dissolution rate should be proportional to the concentration of a protonated surface species (Schott, 1990; Brady and House, 1996). Therefore, the increase of brucite dissolution rate as a function of H^+ activity can be only attributed to the protonation of >MgOH° sites leading to formation of $>MgOH_2^+$. This can be assessed by plotting the forward dissolution rate of brucite at far from equilibrium conditions as a function of $>MgOH_2^+$ concentration calculated using the SCM generated in this study (Fig. 9). For $2.5 \le pH \le 11.5$, a good correlation is observed ($R_{sq} = 0.962$) with a second order dependence of the forward dissolution rate (R_+) on $>MgOH_2^+$ concentration:

$$R_+ = 10^{1.99\pm0.09} \cdot \{>MgOH_2^+\}^{1.90\pm0.02} \quad (5)$$

where the units of R_+ and $\{>MgOH_2^+\}$ are mol/m^2/s and mol/m^2, respectively. This reaction order is consistent with the observation that the reaction order of proton-promoted dissolution rate of simple oxides generally coincides with the charge of the central metal ion (Wieland et al., 1988).

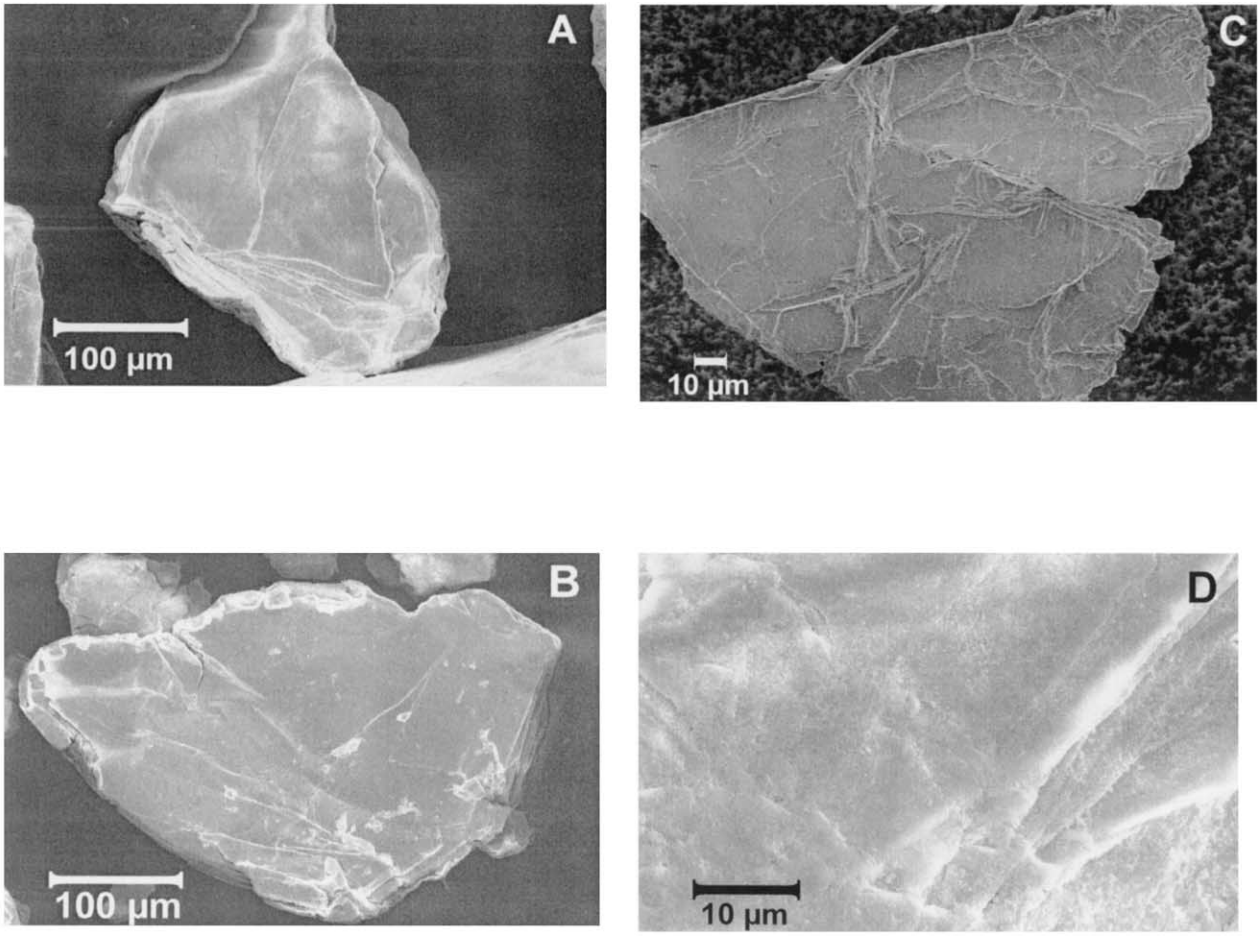

Fig. 7. SEM photomicrographs showing the surface of brucite used in this study: (A) initial grains, (B) after dissolution at pH 7 during 154 h, (C) after dissolution at pH 3.5 during 150 h, and (D) after precipitation at pH 10.8 during 370 h.

3.2.2.2. Dissolution and precipitation at close to equilibrium conditions. According to TST, the same surface precursor complex should control both dissolution and crystallization reactions if a single rate-limiting step controls the overall rate or steady state is reached for each elementary reaction and the magnitude of chemical affinity for each elementary reaction is not much greater than **R**T (Boudart, 1976; Nagy et al., 1991; Nagy and Lasaga, 1992). This appears to be verified for brucite as illustrated by Figure 10 where crystallization rates measured at constant supersaturation index are plotted as a function of the concentration of hydrated Mg centers. Some scatter of brucite precipitation rates in this figure is due to the influence on R_- of chemical affinity that is not exactly the same for each data point. However, a linear correlation with a slope close to 2 is observed:

Table 5. Change of specific surface area during brucite dissolution and precipitation experiments.

No	Duration, h	Grain size (μm)	S_0, m^2/g	S_f, m^2/g	pH	Rate, $mol/m^2/s$
40	27	100–200	0.1200	0.2420	2.5	$1.0 \cdot 10^{-7}$
41	42	100–200	0.1200	0.2830	3.2	$6.6 \cdot 10^{-8}$
42	175	100–200	0.1200	0.2900	6.5	$2.4 \cdot 10^{-8}$
21	160	100–200	0.1200	0.2570	7	$3.6 \cdot 10^{-8}$
7	240	50–100	0.2035	0.3000	10.8	$3.3 \cdot 10^{-10}$
29	310	50–100	0.2035	0.7630	10.9	$-8 \cdot 10^{-10}$
6	350	50–100	0.2035	0.2950	11.0	$1.1 \cdot 10^{-9}$
16	70	100–200	0.1200	0.2130	11.1	$1.8 \cdot 10^{-10}$
37	330	100–200	0.1200	0.1464	11.3	$-1.9 \cdot 10^{-10}$
17	720	100–200	0.1200	0.1790	11.4	$-2.9 \cdot 10^{-11}$
59	260	100–200	0.1200	0.3600	11.9	$-6.8 \cdot 10^{-11}$
5	330	50–100	0.2035	0.3010	11.9	$1.9 \cdot 10^{-11}$
39	330	100–200	0.1200	0.2490	12.1	$-8.0 \cdot 10^{-11}$

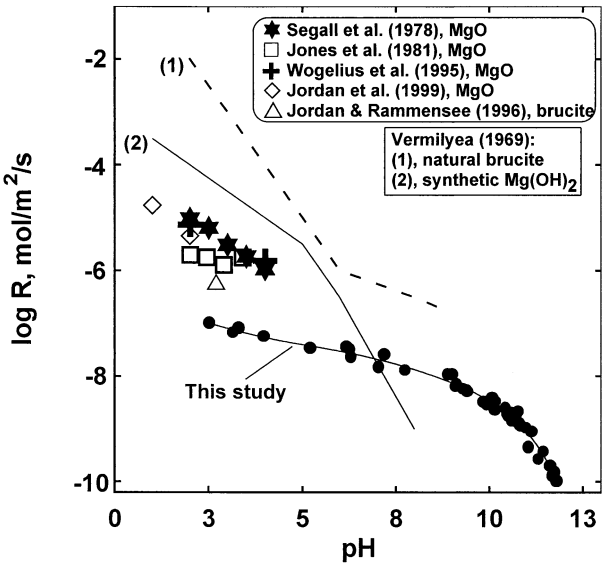

Fig. 8. Summary of literature data on brucite and periclase dissolution rates at 25°C as a function of pH.

$$R_{-} = 10^{3.98\pm0.12} \cdot \{>MgOH_2^+\}^{2.28\pm0.03} \quad (6)$$

where the units of R_- and $\{>MgOH_2^+\}$ are mol/m^2/s and mol/m^2, respectively. Eqn. 5 and 6 suggest that both dissolution and precipitation processes require the hydration of two adjacent magnesium surface sites.

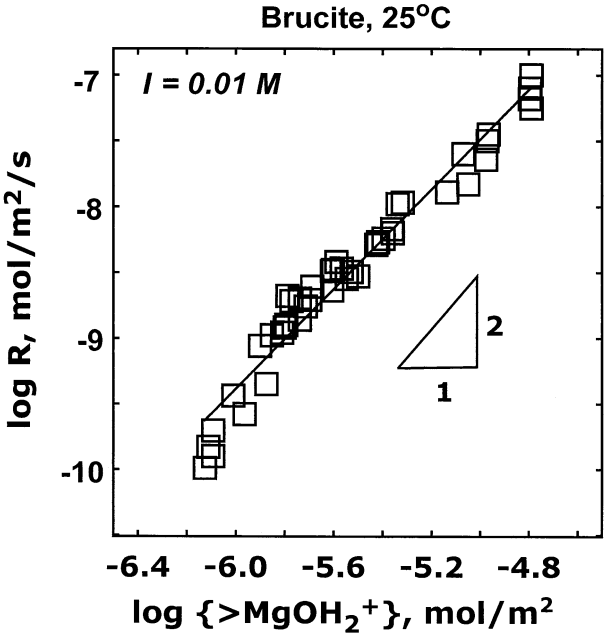

Fig. 9. Brucite dissolution rate at 25°C, pH of 2.5 to 12 and ionic strength of 0.01 mol/L as a function of $\{>MgOH_2^+\}$. The slope of two suggests a surface precursor activated complex composed of two adjacent hydrated Mg sites. The coincidence of the values of slope (n = 2) and the oxidation state of the central metal (Mg^{2+}) is in agreement with surface coordination theory (Wieland et al., 1988).

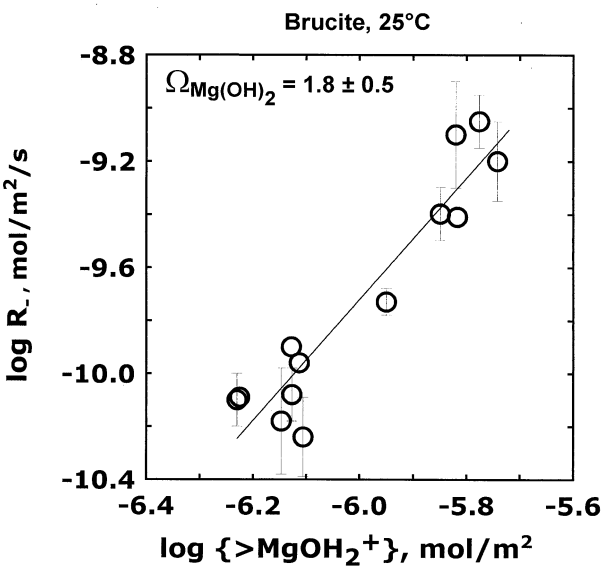

Fig. 10. Brucite precipitation rate at 25°C, constant saturation index (Ω = 1.8 ± 0.5), pH of 10 to 12 and ionic strength of 0.01 to 0.001 mol/L as a function of $\{>MgOH_2^+\}$. In accord with TST predictions, brucite precipitation rate is proportional to the square of the concentration of the rate-controlling surface species, $>MgOH_2^+$.

3.2.3. *Construction and application of a general brucite dissolution/precipitation rate equation*

A general model of brucite dissolution/precipitation kinetics can be obtained within the framework of TST using Eqn. 3 and 4. According to TST, the overall rate (R) of a mineral dissolution reaction per unit surface area can be described using (Lasaga, 1981; Oelkers et al., 1994; Schott and Oelkers, 1995)

$$R = R_+ - R_- = R_+ \cdot [1 - \exp(-A/\boldsymbol{\sigma}\mathbf{R}T)] \quad (7)$$

where R_+ and R_- designate specific forward and backward reaction rates, respectively, **R** is the gas constant, T is the absolute temperature, and $\boldsymbol{\sigma}$ is Temkin's average stoichiometric number equal to the ratio of the rate of activated or precursor complex destruction relative to the overall dissolution rate. A denotes the chemical affinity for the overall hydrolysis reaction given by

$$A = -\boldsymbol{R}T \ln(Q/K^\circ_{sp}) = -\boldsymbol{R}T \ln \Omega \quad (8)$$

where Q is the ion activity quotient, K°_{sp} is brucite thermodynamic solubility product and Ω represents the solution saturation index with respect to this mineral. The forward reaction rate, R_+, is equal to the product of two factors, the concentration of a rate-controlling surface complex, sometimes referred to as precursor complex (P^*), and the rate of destruction of this precursor to form reaction products (Wieland et al., 1988; Stumm and Wieland, 1990; Oelkers et al., 1994). This concept is consistent with

$$R_+ = k_{p^*}[P^*] \quad (9)$$

where k_{p^*} refers to a rate constant compatible with the P^* precursor complex and $[P^*]$ stands for its concentration.

It follows from Eqn. 5 and 6 and Figures 9 and 10 that the

rate controlling step for brucite is the hydration of exposed Mg surface sites. Hydration of n Mg sites leads to precursor complex $[n >MgOH_2^+]^*$ formation according to

$$n{>}MgOH^\circ + nH_2O = [n{>}MgOH_2^+]^* + nOH^- \quad (10a)$$

$$n{>}MgO^- + 2nH^+ = [n{>}MgOH_2^+]^* \quad (10b)$$

For the sake of simplicity, it is assumed that all metal sites contain either $>MgOH^\circ$ or $>MgOH_2^+$ and the percentage of $>MgO^-$ sites is negligible. Combining Eqn. 9 and 10a yields

$$R_+ = k_{Mg}^+ \cdot \{>MgOH_2^+\}^n = k_{Mg}^+ \cdot K^*_+ \cdot \{>MgOH^\circ\}^n \cdot a_{OH^-}^{-n} \quad (11)$$

where K^*_+ is the equilibrium constant of reaction 10a and k_{Mg}^+ is the forward, or dissolution, rate constant.

Assuming that close to equilibrium ($-2 \le A \le 2$ kJ/mol) the surface precursor complex $[n >MgOH_2^+]^*$ is the same for dissolution and precipitation, its reaction formation for precipitation can be expressed as:

$$n{>}MgOH^\circ + nMg^{2+} + 2nH_2O \rightarrow [n{>}MgOH_2^+]^* + nMg(OH)_2(solid) + nH^+ \quad (12)$$

Reactions (9) and (11) lead to an expression for the brucite precipitation rate (R_-) given by

$$R_- = k_{Mg}^-\{ > MgOH_2^+\}^n = k_{Mg}^- \cdot K^*_- \cdot \{>MgOH^\circ\}^n \cdot a_{H_2O}^{2n} \cdot a_{Mg^{2+}}^n \cdot a_{H^+}^{-n} \quad (13)$$

where K*- is the equilibrium constant of reaction 10a. It follows from TST theory that at equilibrium $R_- = R_+$ and thus

$$(k_{Mg}^+ \cdot K^*_+)/(k_{Mg}^- \cdot K^*_-) = (K^\circ_{sp}/K_w)^n \quad (14)$$

where K_w stands for water dissociation constant. Combining Eqn. 7, 9, 11, 13 and 14 yields the following expression for brucite overall reaction rate

$$R_T = k_{Mg}^+\{>MgOH_2^+\}^n \cdot (1 - \Omega^n) \quad (15)$$

where n was approximated as 2.0 ± 0.1 based on dissolution and precipitation data (Eqn. 5 and 6). This equation implies that Temkin's average stoichiometric number ($\boldsymbol{\sigma}$ in Eqn. 7) for brucite dissolution/precipitation is equal to 0.5 (i.e., $\boldsymbol{\sigma} = 1/n$), which means that overall dissolution requires the hydration of two adjacent Mg structural sites.

Brucite overall dissolution and precipitation rates are plotted in Figure 6 as a function of log Ω at $10.6<pH<11.0$ and $11.3<pH<12.1$ and I of 0.001 to 0.01 mol/L. In this figure, the solid lines 1 and 2 correspond to the predictions of Eqn. 15 for pH of 10.8 and 11.5, respectively. A good agreement between measured dissolution and precipitation rates and model predictions can be noted at close to equilibrium conditions. TST prediction of brucite crystallization rates in highly supersaturated solutions ($\Omega \ge 2.5$, i.e., log $\Omega \ge 0.4$) is not possible as surface nucleation may become preponderant and the same precursor complex is not likely to control both dissolution and precipitation. The model developed in this study (Eqn. 15) is a first order approximation amenable to further refinement. In particular, at pH > 12, highly reactive $>MgO^-$ sites whose concentration becomes significant cannot be neglected.

3.3. Transient Rates in pH-jump Experiments

Downward pH-jumps to pH 2 or 3 from neutral and alkaline solutions produced an initial-pH-dependent and reproducible non-steady-state (transient) period of elevated brucite dissolution rate that lasted from several tenths of a minute to one hour. The higher the starting pH precedent to acid conditions, the higher the transient brucite dissolution rate and thus the higher the Mg outlet concentrations (Fig. 11). The excess amount of released magnesium during pH-jumps corresponds to the dissolution of several atomic layers. This transient fast dissolution was reproducible since two separate pH 11 to 3 jumps yielded the same results. It should be emphasized it was not produced by the dissolution of ultra-fine particles or surface defects generated by sample preparation as 2 to 3 successive jumps were performed with the same powder sample. The rapid dissolution of a poorly crystallized $Mg(OH)_2$ phase precipitated on brucite surface as a result of upward pH jumps to neutral or alkaline conditions can be also ruled out since brucite solubility product was never exceeded during pH cycles as confirmed by Mg and pH analysis in outlet solution in the course of experiments.

In the light of Samson and Eggleston's pioneering work on the non-steady-state dissolution of trivalent metal oxides (Samson and Eggleston, 1998, 2000; Samson et al., 2000), the results of our pH-jumps experiments are consistent with the progressive decomposition at acid conditions of highly reactive brucite surface sites generated in alkaline solutions. Insights into the nature of these reactive sites can be obtained by looking at both brucite surface speciation and magnesium aqueous speciation as a function of pH.

3.3.1. Brucite surface speciation

Within the framework of the simple constant capacitance SCM developed in this study (see Fig. 3), it can be seen that increasing the solution pH from 6 to 12 results in a significant build up in the concentration of $>MgO^-$ surface sites. Similar to the role of $>SiO^-$ in quartz and silicate dissolution (Brady and Walther, 1989; Guy and Schott, 1989; Dove 1994), the replacement in the Mg coordination sphere of a water molecule by a negative oxygen donor polarizes and weakens Mg-O bonds in the brucite structure and thus enhances dissolution. As a result, a downward pH-jump should result in a transient enhanced dissolution rate if proton sorption at the brucite surface is faster than the re-equilibration of brucite surface species (transformation of $>MgO^-$ into $>MgOH_2^+$). To check this hypothesis, $\{>MgO^-\}$ was calculated for the initial pH value before the jump, using the SCM established in this study. It can be seen in Figure 12a that a positive linear correlation is observed between the excess of Mg dissolved during pH jumps and $\{>MgO^-\}$.

3.3.2. Mg aqueous speciation

A complementary view of brucite surface speciation can be provided from the analogy between surface and solution equi-

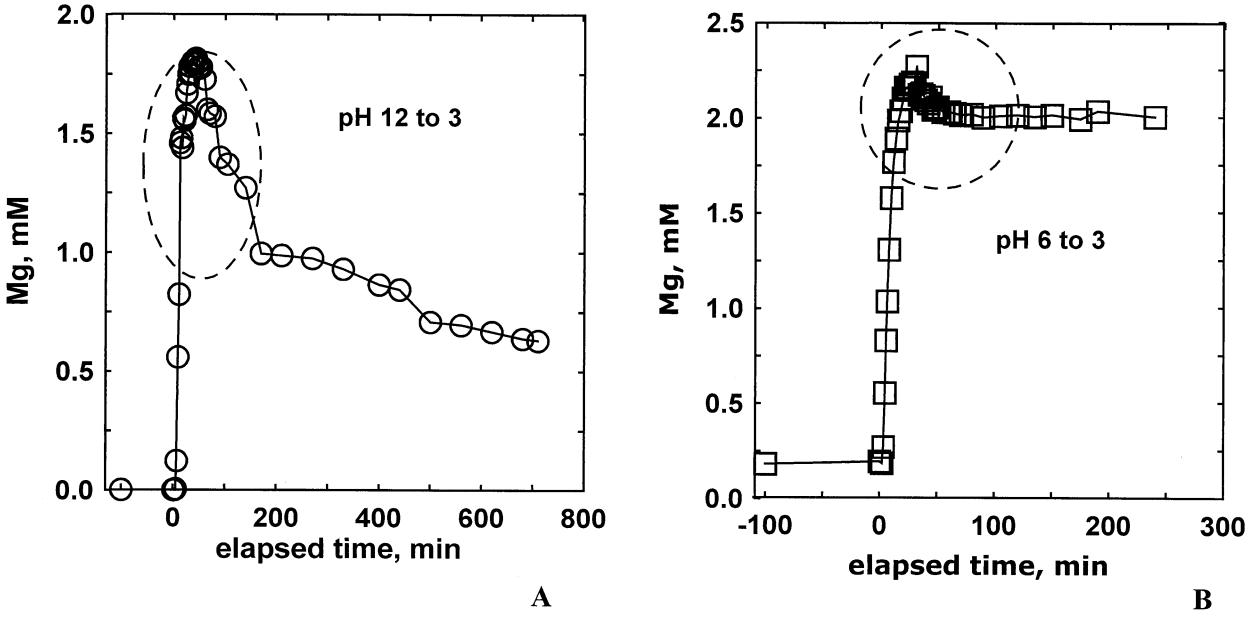

Fig. 11. Examples of pH-jump experiments in 0.01 M NaCl: outlet Mg concentration during pH-jump experiment (A) from pH 12 to pH 3 and (B) from pH 6 to pH 3. Experimental conditions: (A), 0.524 m^2 surface area, flow rate 5.5 mL/min; (B), 0.786 m^2, 4 mL/min.

librium (Schindler and Stumm, 1987). In the case of divalent metals, Pokrovsky and Schott (2002) showed that there is a good positive correlation between the logarithms of stability constants for surface ($>MeOH_2^+$) and solution ($Me(OH)_2°$) metal hydration. It is thus tempting to correlate the excess Mg released in solution to the concentration of $MgOH^+_{(aq)}$, the predominant form of aqueous magnesium at pH>11 (Baes and Mesmer, 1976). Again, a good correlation is observed (Fig. 12b) although it is weaker than that involving {$>MgO^-$}(Fig. 12a).

If correlations shown in Figure 12 cannot serve to define the exact molecular structure of the dissolution-active surface sites generated at alkaline conditions, they nevertheless strongly suggest that these sites are composed of 'hydrolyzed' Mg surface complexes in which one or two water molecules of the Mg coordination sphere have been replaced by hydroxyl (OH^-) or oxo (O^{2-}) ligands. This transformation of surface aquo species into hydroxo and/or oxo complexes can catalyze two important reaction steps involved in mineral dissolution: breaking of crystal Mg-O bonds (formation of the precursor complex) and decomposition (solubilization) of the precursor complex. The weakening of metal-oxygen bonds by the surface coordination with O^{2-} or OH^- has been already stressed above. With regard to the rate limiting solubilization step, Stumm (1992) has shown that, like the rate of metal complex formation in solution, the rate of metal sorption/desorption on an oxide surface (surface complex formation) is proportional to the rate at which water in the inner coordination sphere of the metal ion exchanges with water in the bulk solvent. On the same track it has been shown that the dissolution rates of isostructural orthosilicates (Westrich et al., 1993) and carbonates (Pokrovsky and Schott, 2002) are proportional to the exchange rate of water from the solvent into the hydration sphere of the corresponding dissolved metal. It is thus likely that i) the rate of release of magnesium from brucite surface scales with the water exchange rate from aqueous Mg and ii) the deprotonation of a water molecule in the coordination sphere of surface magnesium following a pH jump should favor dissolution via the resulting increase of the rate of exchange of the remaining water molecules. This labilizing effect of hydrolysis on the rate of ligand exchange has been demonstrated for trivalent metals like Al^{3+} and Fe^{3+} with an increase in the exchange rate of water molecules of about 4 and 3 free orders of magnitude, respectively, following the first deprotonation of their aquo ions (Grant and Jordan, 1981; Nordin et al., 1998). Note that sequential deprotonation steps should further facilitate metal solubilization as well as the replacement of water molecules by ligands containing electron donors.

The results of this study and those reported by Samson et al. (2000) on trivalent oxides point out the limitations of available double layer models in predicting surface speciation solely from titration and electrokinetic measurements. In particular, they demonstrate that the kinetics of sorption of protons (or hydronium ions) on a solid surface is much faster that that of formation or re-equilibration of surface complexes thus contradicting the idea, implicit in the double layer models, that surface protonation occurs directly on the ligands present in the metal coordination sphere, for example transforming hydroxyl groups into water molecules.

4. CONCLUDING REMARKS

The present study illustrates the power of the surface coordination approach in describing the steady state dissolution kinetics of a simple hydroxide mineral at both far from equilibrium and close to equilibrium conditions. When coupled with Transition State Theory at close to equilibrium conditions, this approach allows prediction of brucite crystallization rates

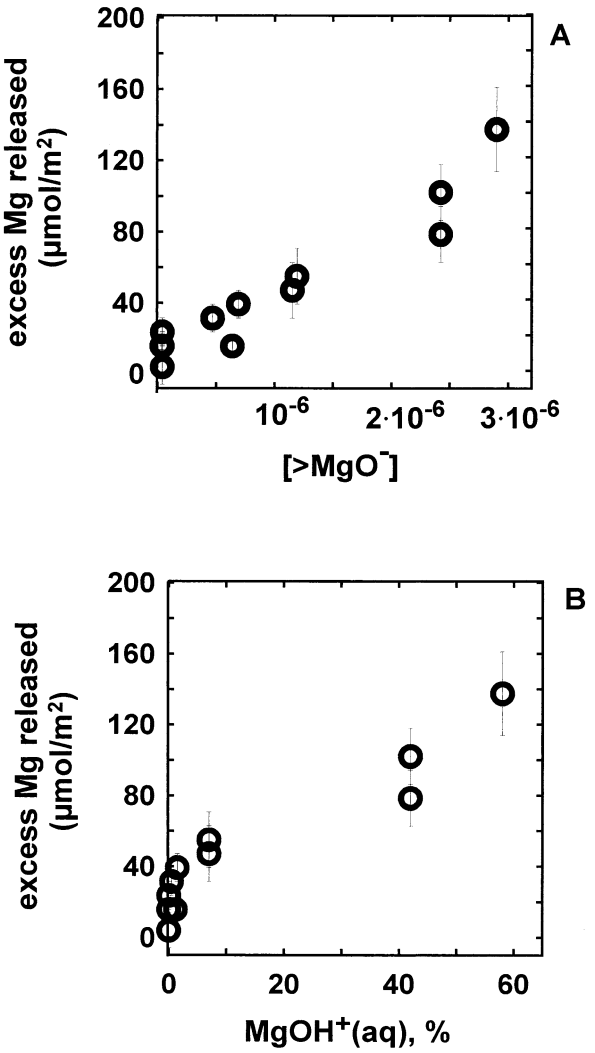

Fig. 12. Excess of Mg released during the pH-jump experiments normalized to the total surface area of solid in reactor as a function of (a) concentration of $>MgO^-$ sites in alkaline solution calculated from the SCM used in this study, and (b) concentration of $MgOH^+$ species in solution.

demonstrating that both dissolution and precipitation are controlled by the formation of the same surface precursor complex, $>MgOH_2^+$. Hydrated magnesium surface centers, and more generally, hydrated divalent metals, were also shown to control the reactivity of carbonates (Pokrovsky and Schott, 2002) and orthosilicates (Westrich et al., 1993; Pokrovsky and Schott, 2000). In this regard, investigation of the dissolution mechanism of other Me^{2+}-bearing silicates (pyroxenes, amphiboles, smectites), phosphates or fluorides will be facilitated by using the results of the present study on brucite.

Study of brucite dissolution at alternate pH conditions (pH-jump experiments) suggests, in accord with previous studies on trivalent metal oxides, that surface metal hydroxylation – leading to the formation of oxo- and hydroxocomplexes – has a labilizing effect on the rates of ligand exchanges at the metal center that favors the production of dissolution-active sites. It is expected that any electron-donor ligands (e.g., OH^-, O^{2-}, F^-, organic acids. . .) can have similar labilizing effects and increase reaction rates when metal hydration is rate controlling. Results of these pH-jump experiments provide new insights into oxide/hydroxide dissolution mechanisms and demonstrate that proton sorption on solid surfaces is much faster than formation or re-equilibration of surface complexes. This calls into question the representation and modeling of surface protonation within the framework of present double layer models. As shown in this study, these models provide an adequate description of oxide/hydroxide steady-state reaction rates but accurate modeling of nonsteady-state rates, i.e., following rapid changes in solution chemistry, would require a better characterization of surface protonation and the nature of proton-bearing complexes using high temporal resolution surface-sensitive spectroscopic tools.

Acknowledgments—The manuscript has greatly benefited from thorough and constructive comments of K. Nagy, G. Jordan, and an anonymous reviewer. The authors are grateful to A. Castillo for performing B.E.T. measurements and careful assistance during pH-jump experiments. D. Okab is thanked for assistance with the SEM analysis. E. Oelkers and Ph. Van Cappellen are thanked for useful discussions.

Associate editor: K. Nagy

REFERENCES

Allison J. D., Brown D. S., and Novo-Gradac K. J. (1991) MINTEAQA2/PRODEFA2, A geochemical assessment model for environmental systems: Version 3.0 user's manual. U.S. EPA, Athens, GA, 106 p.

Altmaier M., Metz V., Neck V., Muller R., and Fanghanel T. (in press) Solid-liquid equilibria of $Mg(OH)_2$(cr) and $Mg_2(OH)_3Cl \cdot 4H_2O$(cr) in the system Mg-Na-H-OH-Cl-H_2O at 25°C. *Geochim. Cosmochim. Acta*.

Amrhein C. and Suarez D. L. (1988) The use of a surface complexation model to describe the kinetics of ligand-promoted dissolution of anorthite. *Geochim. Cosmochim. Acta* **52**, 2785–2793.

Baes C. F., Jr. and Mesmer R. E. (1976) *The Hydrolysis of Cations*. John Wiley & Sons, New York.

Berger G., Cadoré E., Schott J., and Dove P. M. (1994) Dissolution rate of quartz in Pb and Na electrolyte solutions between 25 and 300°C. Effect of the nature of the surface complexes and reaction affinity. *Geochim. Cosmochim. Acta* **58**, 541–551.

Berner R. A. (1991) A model for atmospheric CO_2 over Phanerozoic time. *Am. J. Sci.* **291**, 339–376.

Berry A. J., Fraser D. G., Grime G. W., Craven J., and Sleeman J. T. (1998) The hydration and dissolution of periclase. *Mineral. Magazine* **62A**, 158–159.

Boudart M. (1976) Consistency between kinetics and thermodynamics. *J. Phys. Chem.* **80**, 2869–2870.

Brady P. V. and House W. A. (1996) Surface controlled dissolution and growth of minerals. In *Physics and Chemistry of Mineral Surfaces* (ed. P. V. Brady), pp. 225–306. CRC Press.

Brady P. V. and Walther J. V. (1989) Controls on silicate dissolution rates in neutral and basic pH solutions at 25°C. *Geochim. Cosmochim. Acta* **53**, 2823–2830.

Casey W. H. (1991) On the relative dissolution rates of some oxides and orthosilicate minerals. *J. Colloid Interface Sci.* **146**, 586–589.

Charlet L., Wersin P., and Stumm W. (1990) Surface charge of $MnCO_3$ and $FeCO_3$. *Geochim. Cosmochim. Acta* **54**, 2329–2336.

Chieng C. and Nancollas G. H. (1982) The crystallization of magnesium hydroxide, a constant composition study. *Desalination* **42**, 209–219.

Devidal J.-L., Schott J., and Dandurand J.-L. (1997) An experimental study of kaolinite dissolution and precipitation kinetics as a function of chemical affinity and solution composition at 150 C, 40 bars, and pH 2, 6.8, and 7.8. *Geochim. Cosmochim. Acta* **61**, 5165–5186.

Dove P. M. (1994) The dissolution kinetics of quartz in sodium chloride solutions at 25°C to 300°C. *Am. J. Sci.* **294**, 665–712.

Duval Y., Mielczarski J. A., Pokrovsky O. S., Mielczarski E., and Ehrhardt J. J. (2002) Evidence of the existence of three types of species at the quartz-aqueous solution interface at pH 0–10: XPS surface group quantification and surface complexation modeling. *J. Phys. Chem. B* **106**, 2937–2945.

Fenter P., Geissbuhler P., DiMasi E., Srajer G., Sorensen L. B., and Sturchio N. C. (2000) Surface speciation of calcite observed in situ by high-resolution X-ray reflectivity. *Geochim. Cosmochim. Acta* **64**, 1221–1228.

Gautier J.-M., Oelkers E. H., and Schott J. (1994) Experimental study of K-feldspar dissolution rates as a function of chemical affinity at 150 C and pH 9. *Geochim. Cosmochim. Acta* **58**, 4549–4560.

Grant M. and Jordan R. B. (1981) Kinetics of solvent water exchange on iron (III). *Inorg. Chem.* **20**, 55–60.

Guy C. and Schott J. (1989) Multisite surface reaction versus transport control during the hydrolysis of a complex oxide. *Chem. Geol.* **78**, 181–204.

Hayes K. F., Redden G., Ela W., and Leckie J. O. (1991) Surface complexation models: An evaluation of model parameters estimation using FITEQL and oxide mineral titration data. *J. Colloid. Interface Sci.* **142**, 448–469.

Hostetler P. B. (1963) The stability and surface energy of brucite in water at 25°C. *Am. J. Science* **261**, 238–258.

Huertas F. J., Chou L., and Wollast R. (1998) Mechanism of kaolinite dissolution at room temperature and pressure: Part 1. Surface speciation. *Geochim. Cosmochim. Acta* **62**, 417–431.

Hunter R. J. (1989) *Foundation of Colloid Science*, **Vol. 1**, Clarendon Press, Oxford.

Jones C. F., Segall R. L., Smart S. C., and Turner P. S. (1981) Initial dissolution kinetics of ionic oxides. *Proc. R. Soc. London A* **374**, 141–153.

Jones C. F., Reeve R. A., Rigg R., Segall R. L., Smart R. S. C., and Turner P. S. (1984) Surface area and the mechanism of hydroxylation of ionic oxide surfaces. *J. Chem. Soc. Faraday Trans. I* **80**, 2609–2617.

Jordan G. and Rammensee W. (1996) Dissolution rates and activation energy for dissolution of brucite (001): A new method based on the microtopography of crystal surfaces. *Geochim. Cosmochim. Acta* **60**, 5055–5062.

Jordan G., Higgins S. R., and Eggleston C. M. (1999) Dissolution of the periclase (001) surface: A scanning force microscopy study. *American Mineralogist* **84**, 144–151.

Klein D. H., Smith M. D., and Driy J. A. (1967) Homogeneous nucleation of magnesium hydroxide. *Talanta* **14**, 937–940.

Knauss K. G., Nguyen S. N., and Weed H. C. (1993) Diopside dissolution kinetics as a function of pH, CO_2, temperature, and time. *Geochim. Cosmochim. Acta* **57**, 285–294.

Kramer S. M. and Hering J. G. (1997) Influence of solution saturation state on the kinetics of ligand-controlled dissolution of oxide phases. *Geochim. Cosmochim. Acta* **61**, 2855–2866.

Lasaga A. C. (1981) Transition State Theory. In *Kinetics of Geochemical Processes* (ed. A. C. Lasaga and R. J. Kirkpatrick), *Rev. Mineral.* **8**, 135–169.

Liu S.-T. and Nancollas G. H. (1973) The crystallization of magnesium hydroxide. *Desalination* **12**, 75–84.

MacDonald D. D. and Owen D. (1971) The dissolution of magnesium oxide in dilute sulfuric acid. *Canad. J. Chem.* **49**, 3375–3380.

Monastra V. and Grandstaff D. E. (1999) Kinetics of MgO dissolution and buffering fluids in the Waste Isolation Pilot Plant (WIPP) repository. *Mat. Res. Soc. Symp. Proc.* **556**, 625–632.

Morth C.-M, and Strandh H. (1999) Brucite dissolution at pH 1.74 to 4.7 at 25°C to 55°C. *Proceed. Internat. Conf. Geochemistry of the Earth Surface*, Reykjavik, 1999, p. 457–460.

Nagy K. L. and Lasaga A. C. (1992) Dissolution and precipitation kinetics of gibbsite at 80° C and pH 3: The dependence on solution saturation state. *Geochim. Cosmochim. Acta* **56**, 3093–3111.

Nagy K. L., Blum A., and Lasaga A. C. (1991) Dissolution and precipitation kinetics of kaolinite at 80°C and pH 3: The dependence on solution saturation state. *Am. J. Sci.* **291**, 649–686.

Nordin J. P., Sullivan D. J., Phillips B. L., and Casey W. H. (1998) An ^{17}O – NMR study of the exchange of water on $AlOH(H_2O)_5^{2+}$(aq). *Inorg. Chem.* **37**, 4760–4763.

Oelkers E. H. (2001) General kinetic description of multioxide silicate mineral and glass dissolution. *Geochim. Cosmochim. Acta* **65**, 3703–3719.

Oelkers E. H. and Schott J. (2001) An experimental study of enstatite dissolution rates as a function of pH, temperature, and aqueous Mg and Si concentration, and the mechanism of pyroxene/pyroxenoid dissolution. *Geochim. Cosmochim. Acta* **65**, 1219–1231.

Oelkers E. H., Schott J., and Devidal J.-L. (1994) The effect of aluminum, pH, and chemical affinity on the rates of aluminosilicate dissolution reactions. *Geochim. Cosmochim. Acta* **58**, 2011–2024.

Palmer D. A. and Wesolowski D. J. (1997) Potentiometric measurements of the first hydrolysis quotient of magnesium(II) to 250°C and 5 molal ionic strength (NaCl). *J. Solution Chem.* **26**, 217–232.

Phillips V. A., Kolbe J. L., and Opperhauser H. (1977) Effect of pH on the growth of $Mg(OH)_2$ crystal in an aqueous environment at 60°C. *J. Crystal Growth* **41**, 228–234.

Pokrovsky O. S. and Savenko V. S. (1992) Experimental determination of magnesium activity coefficient in seawater. *Oceanology* **32,** *6*, 724–730.

Pokrovsky O. S. and Schott J. (1999) Processes at the magnesium-bearing carbonates/solution interface. II. Kinetics and mechanism of magnesite dissolution. *Geochim. Cosmochim. Acta* **63**, 881–897.

Pokrovsky O. S. and Schott J. (2000) Kinetics and mechanism of forsterite dissolution at 25°C and pH from 1 to 12. *Geochim. Cosmochim. Acta* **64**, 3313–3325.

Pokrovsky O. S. and Schott J. (2002) Surface chemistry and dissolution mechanism of divalent metal carbonates. *Environ. Sci. Technol.* **36**, 426–432.

Pokrovsky O. S., Schott J., and Thomas F. (1999a) Processes at the magnesium-bearing carbonates/solution interface. I. A surface speciation model for magnesite. *Geochim. Cosmochim. Acta* **63**, 863–880.

Pokrovsky O. S., Schott J., and Thomas F. (1999b) Dolomite surface speciation and reactivity in aquatic systems. *Geochim. Cosmochim. Acta* **63**, 3133–3143.

Samson S. D. and Eggleston C. M. (1998) Active sites and the non-steady-state dissolution of hematite. *Environ. Sci. Technol.* **32**, 2871–2875.

Samson S. D. and Eggleston C. M. (2000) The depletion and regeneration of dissolution-active sites at the mineral-water interface: II. Regeneration of active sites on α–Fe_2O_3 at pH 3 and pH 6. *Geochim. Cosmochim. Acta* **64**, 3675–3683.

Samson S. D., Stillings L. L., and Eggleston C. M. (2000) The depletion and regeneration of dissolution-active sites at the mineral-water interface: I. Fe, Al, and In sesquioxides. *Geochim. Cosmochim. Acta* **64**, 3471–3484.

Sangwal K. and Arora S. K. (1978) Etching of MgO crystals in acids: Kinetics and mechanism of dissolution. *J. Material Sci.* **13**, 1977–1985.

Schindler P. W. and Stumm W. (1987) The surface chemistry of oxides, hydroxides, and oxide minerals. In *Aquatic Surface Chemistry* (ed. W. Stumm), pp. 337–365. Wiley.

Schott H. (1981) Electrokinetic studies of magnesium hydroxide. *J. Pharmac. Sci.* **70**, 486–489.

Schott J. (1990) Modeling of the dissolution of strained and unstrained multiple oxides: The surface speciation approach. In *Aquatic Chemical Kinetics* (ed. W. Stumm), pp. 337–365, J. Wiley & Sons.

Schott J. and Berner R. A. (1983) X-ray photoelectron studies of the mechanism of iron silicate dissolution during weathering. *Geochim. Cosmochim. Acta* **47**, 2233–2240.

Schott J. and Berner R. A. (1985) Dissolution mechanisms of pyroxenes and olivines during weathering. In *The Chemistry of Weathering* (ed. J. J. Drever), pp. 35–53, D. Riedel.

Schott J. and Oelkers E. (1995) Dissolution and crystallization of silicate minerals as a function of chemical affinity. *Pure Appl. Chem.* **67**, 903–910.

Schott J., Berner R. A., and Sjöberg E. L. (1981) Mechanism of pyroxene and amphibole weathering - I. Experimental studies of iron-free minerals. *Geochim. Cosmochim. Acta* **45**, 2123–2135.

Segall R. L., Smart R. S. C., and Turner P. S. (1978) Ionic oxides: Distinction between mechanisms and surface roughening effects in the dissolution of magnesium oxide. *J. Chem. Soc. Faraday Trans. I* **74**, 2907–2912.

Stumm W. (1992) *Chemistry of the Solid-Water Interface.* Wiley.

Stumm W. (1997) Reactivity at the mineral-water interface: Dissolution and inhibition. *Colloids Surfaces, A: Physicochem. Eng. Aspects* **120**, 143–166.

Stumm W. and Wieland E. (1990) Dissolution of oxide and silicate minerals: Rates depend on surface speciation. In *Aquatic Chemical Kinetics: Reaction Rates of Processes in Natural Waters* (ed. W. Stumm), pp. 367–400, J. Wiley & Sons.

Sverjensky D. A. and Sahai N. (1996) Theoretical prediction of single-site surface-protonation equilibrium constants for oxides and silicates in water. *Geochim. Cosmochim. Acta* **60**, 3773–3797.

Tsuge H., Okada K., Yano T., Fukushi N., and Akita H. (1997) Reactive crystallization of magnesium hydroxide. Separation and Purification by Crystallization. *ACS Symposium Series* **667**, 254–266.

Van Cappellen P., Charlet L., Stumm W., and Wersin P. (1993) A surface complexation model of the carbonate mineral - aqueous solution interface. *Geochim. Cosmochim. Acta* **57**, 3505–3518.

Velbel M. A. (1999) Bond strength and the relative weathering rates of simple orthosilicates. *Am. J. Sci.* **299**, 679–696.

Vermilyea D. A. (1969) The dissolution of MgO and $Mg(OH)_2$ in aqueous solutions. *J. Electrochem. Soc.* **116**, 1179–1183.

Westrich H. R., Cygan R. T., Casey W. H., Zemitis C., and Arnold G. W. (1993) The dissolution kinetics of mixed-cation orthosilicate minerals. *Am. J. Sci.* **293**, 869–893.

Wieland E., Wehrli B., and Stumm W. (1988) The coordination chemistry of weathering: III. Generalization of the dissolution rates of minerals. *Geochim. Cosmochim. Acta* **52**, 1969–1981.

Wogelius R. A. and Walther J. V. (1991) Olivine dissolution at 25°C: Effects of pH, CO_2, and organic acids. *Geochim. Cosmochim. Acta* **55**, 943–954.

Wogelius R. A., Refson K., Fraser D. G., Grime G. W., and Goff J. P. (1995) Periclase surface hydroxylation during dissolution. *Geochim. Cosmochim. Acta* **59**, 1875–1881.

Wu L., Forsling W., and Schindler P. W. (1991) Surface complexation of calcium minerals in aqueous solution. 1. Surface protonation at fluorapatite - water interface. *J. Colloid. Interface Sci.* **147**, 178–185.